Optics and Feed Design for the wSMA Receiver System

Paul K. Grimes, Scott N. Paine, Lingzhen Zeng, and Edward C.-Y. Tong.

Abstract— **We are currently developing a major upgrade for the Submillimeter Array (SMA) receiver systems, which will involve the complete replacement of receiver cryostat, cartridges, front-ends, and receiver optics with a newly designed receiver system. This upgrade, known as the "wideband SMA" (wSMA) will enable a substantial increase in the instantaneous bandwidth of the SMA to at least 16 GHz per sideband [1]. The upgrade will bring significant improvements in sensitivity and polarimetric performance, and will include provision for future upgrades.**

The new receiver system improves upon the previous SMA receiver optics, eliminating several room temperature receiver optics elements as well as the cooled receiver lenses, and introducing dual-polarized feedhorns which will greatly aid in polarimetric observations.

We present the methods used to design, optimize and tolerance the new receiver optics, starting from the imaging beam waveguide conditions and working through Gaussian beam analysis and simulation of the optical system with physical optics. We also describe the design of the new feeds for the wSMA system.

Index Terms—**Antennas, feeds, quasioptics, radio astronomy, submillimeter astronomy.**

I. Introduction

THE Submillimeter Array (SMA) was conceived three decades ago as the world's first submillimeter interferometer capable of sub-arcsecond imaging in the frequency range from 200 to 700 GHz. Since it began full science operations in 2004 it has been continuously upgraded with new receiver cartridges, expanded intermediate frequency (IF) bandwidth, and augmented polarimetric and dual frequency observing modes. The next step in the development of the SMA is called the wideband Submillimeter Array (wSMA). The wSMA upgrade [1] will replace the original SMA cryostats, receivers, and receiver selection optics with all new systems, and incorporate a number of major upgrades to the backend IF signal transport and correlator systems. This will enable the wSMA to operate with 32 GHz instantaneous bandwidth per receiver polarization, and will form the basis of future development efforts.

The new wSMA receiver optics design is substantially different to that of the SMA receiver optics, with the replacement of room temperature and transmissive optics with cooled reflective optics, the elimination of quasioptical local oscillator (LO) injection, and major changes to the receiver selection mechanism. The new wSMA receiver optics are designed to couple to the SMA antennas' existing beam waveguide, with no changes to the antenna or beam waveguide.

In this paper, we present the design procedures and goals used in developing the wSMA receiver optics design, and the design procedures used to develop the new feeds for the receiver frontend modules. The initial design of the receiver optics was developed using the imaging beam waveguide conditions described by Chu [4], and then further refined using Gaussian beam analysis before carrying out physical optics simulations of the complete wSMA system from feed to sky using TICRA's GRASP software package, with the feeds being analyzed and optimized using both TICRA's CHAMP software and custom modal matching software. Custom software packages were developed in Python to analyze the GRASP and CHAMP outputs.

II. SMA Optical Design

The SMA antennas are of a bent Nasmyth design, fed by a beam waveguide that places the receiver feed horn aperture at an image of the antenna aperture (Fig. 1) [2]. This allows for frequency-independent illumination of the 6 m aperture from a

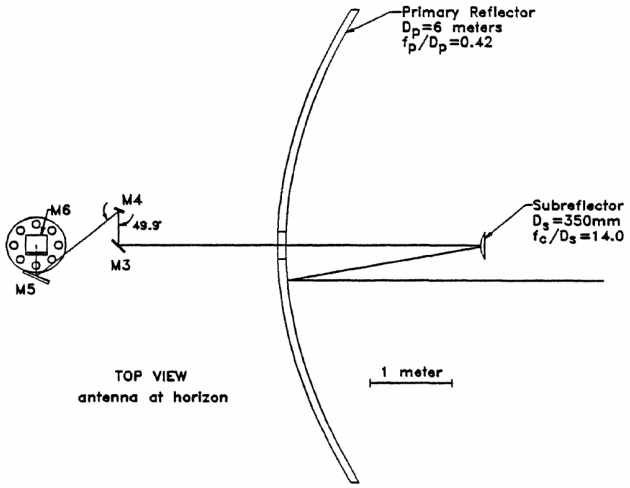

Fig. 1. Layout of the SMA antenna and beam waveguide, taken from [3]. M3 to M6 form the SMA beam waveguide, feeding the receiver system on the far left of the diagram.

The Submillimeter Array is a joint project between the Smithsonian Astrophysical Observatory and the Academia Sinica Institute of Astronomy and Astrophysics and is funded by the Smithsonian Institution and the Academia Sinica.

Paul K. Grimes, Scott N. Paine, Lingzhen Zeng, and Edward C.-Y. Tong are with the Center for Astrophysics | Harvard & Smithsonian, Cambridge, MA 02138, USA (e-mail: pgrimes@cfa.harvard.edu).

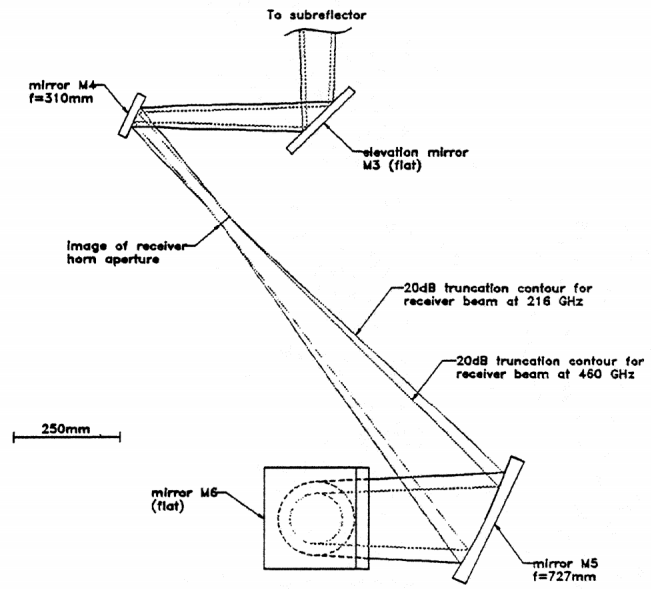

Fig. 2. Details of the SMA beam waveguide, taken from [3]. A movable calibration load and rotating quarter waveplates can be inserted at the image of the receiver horn aperture between M4 and M5.

feed with a frequency-independent aperture field distribution. In order to maximize the gain of the antennas, a 10 dB edge-taper is chosen.

The current SMA antennas use four common mirrors in the beam waveguide (M3/"tertiary" to M6, Fig. 2) to feed a moving wire grid and combiner mirror pair that split and direct orthogonal polarizations to two of four receiver optics inserts

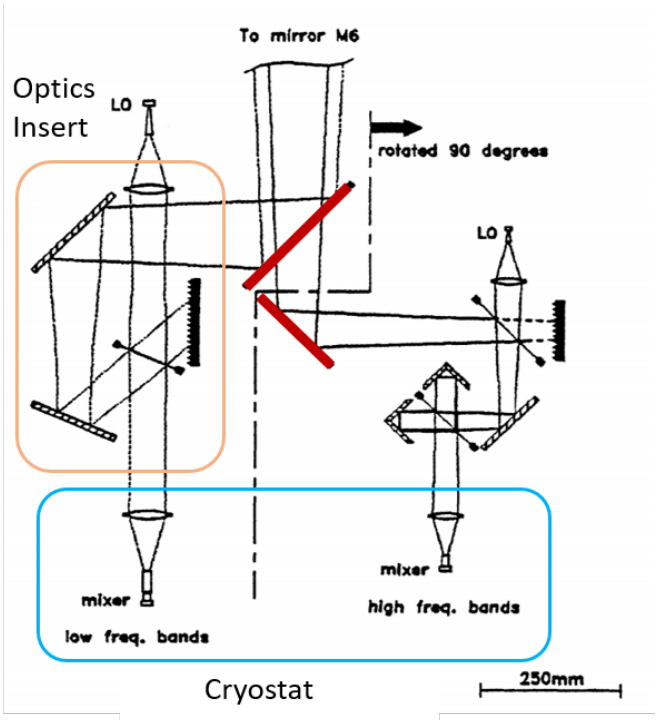

Fig. 3. The current SMA cryostat optical layout from [3], showing the moving grid and mirror receiver selectors (red), the room temperature LO injection optics in the Optics Insert (orange) and the cold receiver cartridge Teflon lens and feed horn. The right hand Optics Insert shows a Martin-Puplett diplexer LO injection scheme which was only used with the obsolete 690 GHz receivers.

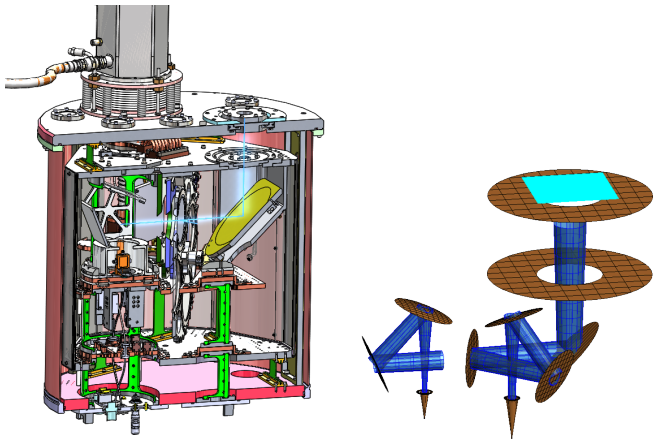

Fig. 4. (right) Cut-away CAD rendering of the wSMA cryostat, showing the cryostat structure and the optical layout (optical path highlighted in blue on the left image). (left) GRASP model of the wSMA cryostat optics, with the Gaussian beam from each feed shown in blue. Rendering courtesy of HPD Inc.

and receiver cartridges (Fig. 3). The optics inserts fold the beam before coupling LO power into the sky signal via a 99% reflective mesh. The beam then enters the receiver cartridge and is focused onto the feed horn by a Teflon lens cooled to ~80 K.

Careful alignment of the feed, receiver lens and optics inserts, and positioning of the combiner grid and mirrors is required in order to achieve coalignment of all receivers on the sky. This is of particular importance for polarimetric observations, as two orthogonally polarized signals travel through independent combiners, optical inserts, receiver lens and feeds, and misalignment can significantly affect the effective sensitivity of the antenna.

III. wSMA Optical Design

The new wSMA receivers will replace all of the optics from the wire grid to the receiver feeds. The beam from M6 enters the cryostat through a vacuum window and an IR filter on the 50 K radiation shield before being reflected through 90° by a plane mirror (Fig. 4). The beam then passes to a movable receiver "selector wheel", where it is either reflected to the low frequency receiver cartridge (210-270 GHz LO) or transmitted to the high frequency receiver cartridge (280-360 GHz LO). The selector wheel will also contain both a wire grid and a dichroic element to enable dual frequency observing in one of two possible polarization modes – either with one polarization per receiver cartridge or with both receiver cartridges dual polarized, with the latter mode processed at half the standard on-sky bandwidth. Both the fold mirror and selector wheel are mounted on the 50 K radiation shield top plate.

Each receiver cartridge will have a pair of "Receiver Optics" mirrors in a clam-shell arrangement that takes the incoming beam from the selector wheel and focuses it onto the dual-polarized receiver feed horn. The use of dual-polarized feeds ensures coalignment on the sky between the two orthogonally polarized beams.

The receiver optics and receiver front-end modules are mounted on a floating 4K cold-plate, which is aligned to the 50 K radiation shield top plate when the cartridge is inserted.

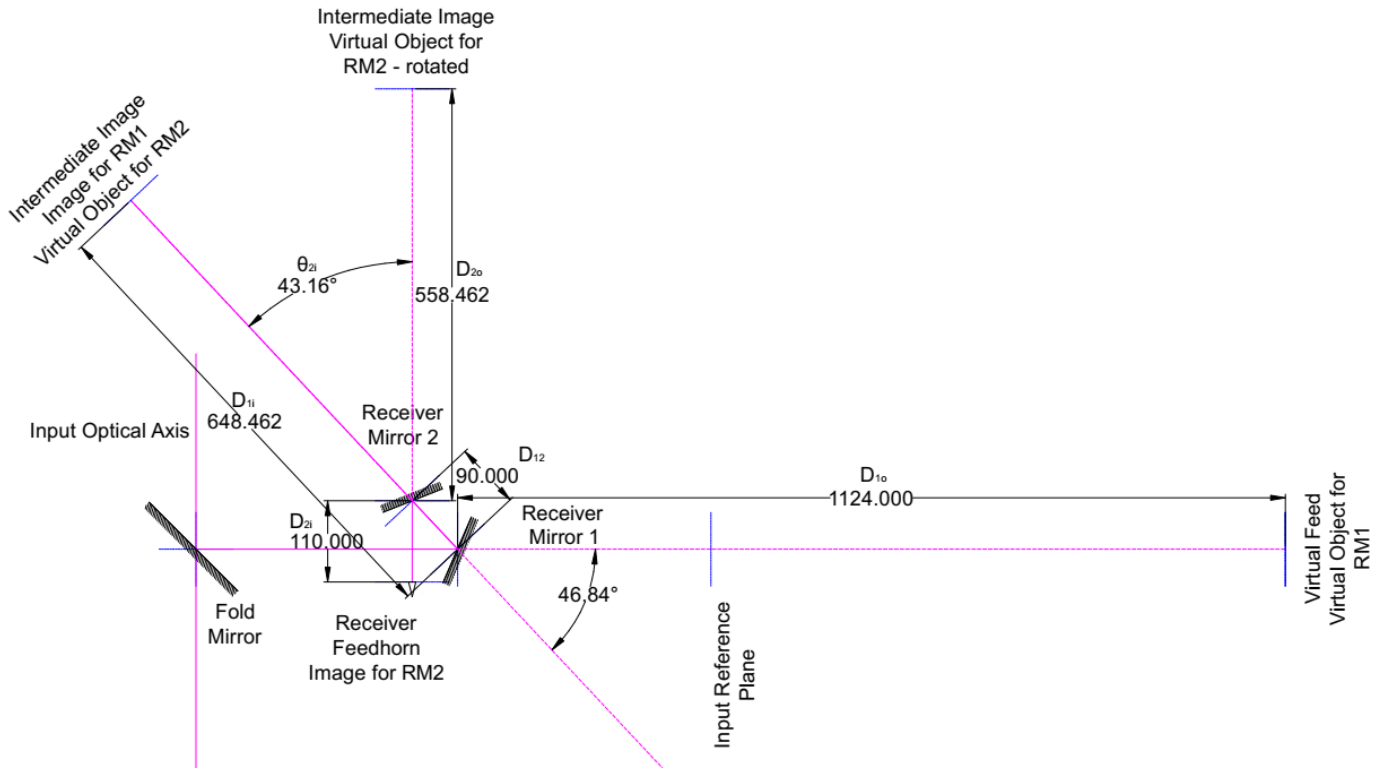

Fig. 5. The wSMA receiver optics layout, with dimensions used in the imaging calculations.

The 50 K top plate thus serves as a common mechanical alignment reference for all of the optical elements.

IV. Imaging Beam Waveguide Design

An imaging beam waveguide is a sequence of optical elements designed to provide frequency-independent matching between the input and output field distributions [4]. The frequency-independent Fresnel imaging equations provide a tool to design the optical system so that a frequency-independent match is obtained between input and output Gaussian beams (or any other field distribution).

The existing SMA beam waveguide was designed [3] to place a frequency-independent virtual feed below each SMA receiver lens and feed, defined by its Gaussian beam radius and radius of phase curvature. The receiver lens reimages this virtual feed on the feedhorn aperture. Different receiver lens focal lengths and feedhorn apertures were chosen for each frequency band used in the SMA.

For the wSMA receivers, the fold mirror and selector wheel will direct the beam to each of the receiver cartridges, entering the receiver optics from the side and placing a virtual feed behind each of the receiver optics assemblies. Because we no longer need to fold the beam to inject the local-oscillator signal, the receiver optics intercept the beam further in front of the virtual feed. As the wSMA receivers cover a narrower total frequency range than those originally designed for the SMA, we adopt the same feed aperture and receiver optics design for both receiver bands, allowing receiver optics assemblies to be interchangeable between receiver bands.

Both mirrors in the clamshell pair are offset hyperboloidal mirrors. The first mirror reimages the virtual feed to an intermediate image in front of the first mirror and behind the second mirror. The second mirror then reimages the intermediate image to the feed aperture. The layout of the reimaging system is shown in Fig. 5.

As a convenience to allow existing SMA receiver feeds to be used with the wSMA receiver optics, we constrain the total magnification of the mirror pair (i.e. the scaling from the virtual feed beam radius to the feed beam radius) to be the same as that used for the SMA 300 GHz and 400 GHz receivers:

$$\text{Total Magnification: } m = m_1 \cdot m_2 = 0.11363636 \quad (1)$$

$$\text{Magnification of RM1: } m_1 = -\frac{d_{1i}}{d_{1o}} \quad (2)$$

$$\text{Magnification of RM2: } m_2 = -\frac{d_{2i}}{d_{2o}} \quad (3)$$

The position along the incoming beam at which the first mirror is placed is roughly determined by the overall physical layout of the optics, the need for compactness in order to fit within the cryostat, and the need to fit the cryostat within the receiver cabin.

The distances between the two mirrors and between the second mirror and the feed are chosen to avoid truncation of the beam by the edge of the second mirror or the feed, and to place the angles of reflection close to 45°. The beam widths are estimated from the single-mode Gaussian beam analysis of the beam waveguide described below, resulting in the following dimensions, as well as the relation between the image distance for RM1 and the object distance for RM2:

$$\text{Distance between RM2 and feed: } d_{2i} = 110 \text{ mm}$$
$$\text{Distance between mirrors: } d_{12} = 90 \text{ mm}$$

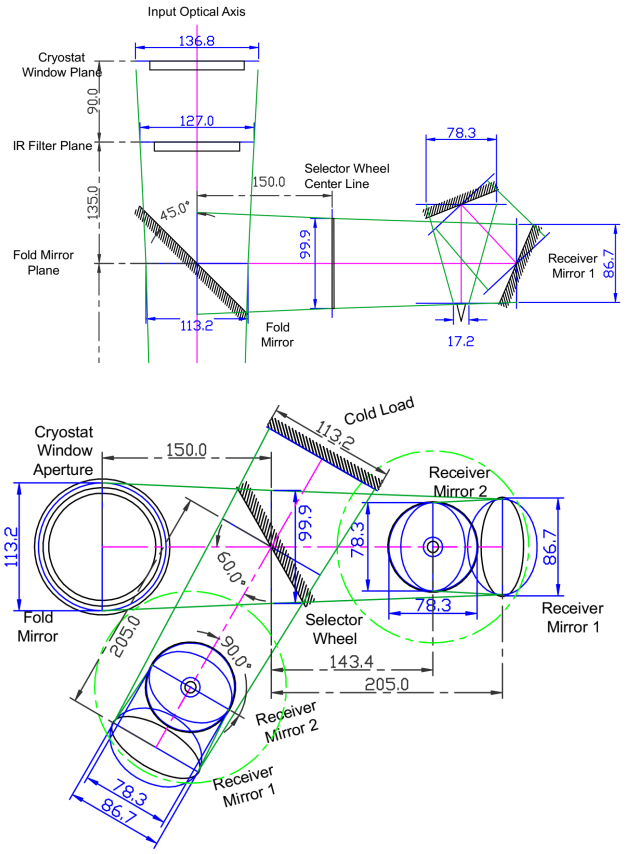

Fig. 6. The wSMA cryostat optical layout, from the side and above, showing the beam widths (blue dimensions) at each of the optical elements.

$$d_{2o} = d_{12} - d_{1i} \tag{4}$$

The position of the intermediate image is then determined by the above imaging equations subject to the constraint set by the chosen overall magnification, with the distance from the first mirror to the virtual feed

$$d_{1o} = 1124 \text{ mm}$$

as the driving parameter.

Solving the equations (1-4) for the intermediate image position, d_{1i}, we obtain:

$$d_{1i} = \frac{m \cdot d_{1o} \cdot d_{12}}{(d_{2i} + m \cdot d_{1o})} = 648.462 \text{ mm} \tag{5}$$

This in turn determines the input object for the second mirror and thus the individual magnifications of the two mirrors.

The precise angles of the mirrors are then set according to the Mizuguchi-Dragone condition:

$$\frac{(1 - m_1)}{m_1} \cdot \tan\theta_1 = (1 - m_2) \cdot \tan\theta_2 \tag{6}$$

which relates the individual reflection angles and magnifications of the two mirrors so that cross-polarization of the beam is minimized. By adding the constraint that the total reflection angle be 90°, the optical system is then fully determined.

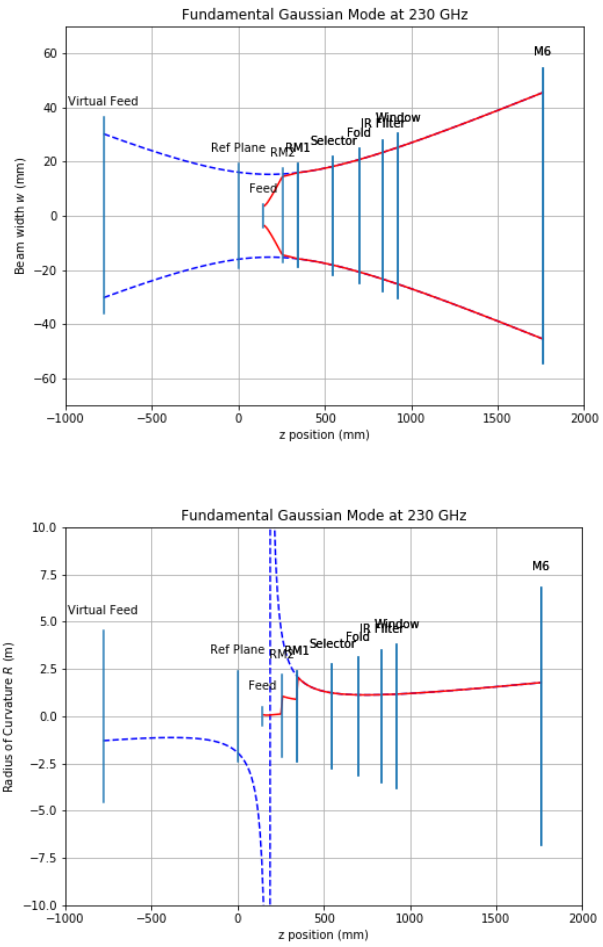

Fig. 7. Results of fundamental mode Gaussian beam analysis of the wSMA receiver optics. The beam from the SMA beam waveguide to the virtual feed is shown with dark blue dashes, while the beam as modified by the wSMA receiver optics is shown in red.

V. Gaussian Beam Analysis

Following the definition of the receiver mirrors using the imaging equations above, a single-moded Gaussian beam analysis of the optical system is used to determine the Gaussian beam radius and radius of phase curvature at the feed aperture, and to check that the mirrors in the system are at least $5w$ in diameter, in order to avoid excessive truncation [5].

The solution of the imaging equations and the Gaussian beam analysis were implemented in a SMath workbook and confirmed using the Gaussian beam propagation software originally developed for designing the SMA optics. The position of the first mirror d_{1o} and the overall optical layout had to be adjusted to give a positive radius of phase curvature at the feed aperture.

The evolution of the Gaussian beam parameters as they pass through the optical system are shown in Fig. 7.

VI. Feed Design

The feeds for the wSMA system are cylindrically symmetric corrugated horns feeding square waveguide inputs to the receiver orthomode transducers. The magnification of the

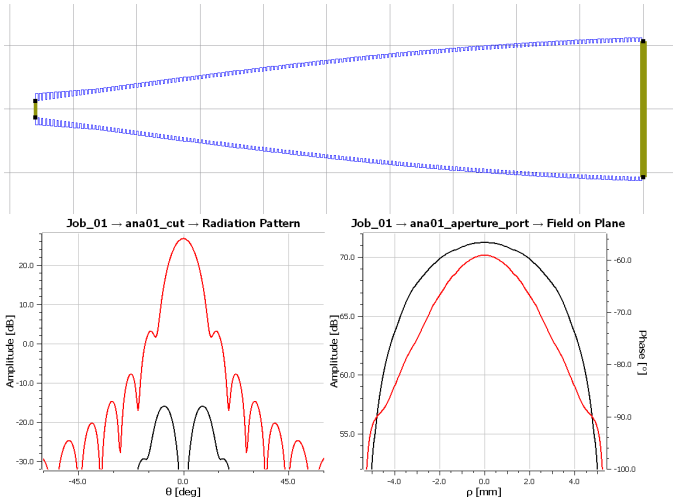

Fig. 8. (top) Optimized corrugated horn profile for the wSMA Low band (210-270 GHz) feed horn. (bottom left) Far-field E-plane radiation pattern at 230 GHz for the horn, showing co-polarized (red) and cross-polarized (black) fields. (bottom right) Aperture field amplitude (black) and phase (red) at 239 GHz for the co-polar E-plane field.

receiver optics was chosen to give the same Gaussian beam radius at the feed aperture as used by the SMA 300 GHz receiver's conical corrugated horn, and this horn serves as the starting point for the wSMA feed designs.

The Gaussian beam analysis above gives the Gaussian beam radius and radius of phase curvature at the horn aperture that must be matched by the wSMA feeds:

$$w = 3.4375 \text{ mm}$$
$$R = 159.64 \text{ mm}$$

Implementing such a horn using a traditional conical corrugated horn profile would require the horn to be prohibitively long, and so a curved horn profile is used.

Initial design of candidate horns were carried out in TICRA's CHAMP software, using modal-matching on CHAMP's built-in sinusoid and asymmetric sine-squared profiles, and variable-depth-slot mode converter designs, described in [6]. Output from the CHAMP software was analyzed in a Jupyter Python Notebook to obtain an estimate of the best fit fundamental Gaussian mode beam radius and radius of phase curvature for the aperture field.

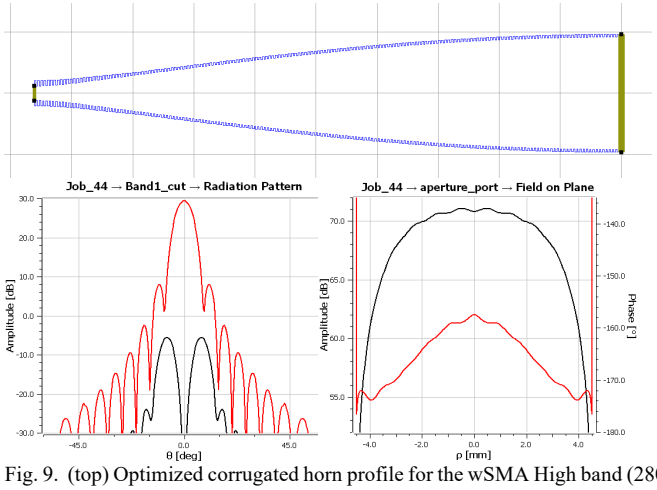

Fig. 9. (top) Optimized corrugated horn profile for the wSMA High band (280-360 GHz) feed horn. (bottom left) Far-field E-plane radiation pattern at 345 GHz for the horn, showing co-polarized (red) and cross-polarized (black) fields. (bottom right) Aperture field amplitude (black) and phase (red) at 345 GHz for the co-polar E-plane field.

The candidate horn designs were then further refined using modal-matching horn analysis software that has been designed to run massively parallel optimizations of horn designs, using a variant of Powell's minimization method [7] and a genetic algorithm. Additional goal functions that allow the complex aperture field mismatch to the fundamental Gaussian mode to be minimized were implemented for this project.

Finally, the optimized horn profiles were input back into TICRA CHAMP, and simulated as a complete feed horn consisting of the square-to-circular waveguide transition, mode-convertor, profiled corrugated horn and the cylindrically symmetric horn outside surface.

Final profiles, far-field beam patterns and aperture field distributions are shown for the Low band and High band feeds in Fig. 8 and Fig. 9 .

The output far-field beam patterns from CHAMP were then used in the GRASP physical optics simulations described in the next section. The GRASP calculated primary aperture illumination and efficiency of the complete wSMA optical system were then used to select the final horn designs.

VII. Physical Optics

Physical optics simulations of the complete SMA and wSMA optical system were implemented in TICRA's GRASP software. These physical optics simulations allowed a direct comparison to be made between the optical performance of the existing SMA receiver system and that of the proposed wSMA receiver system.

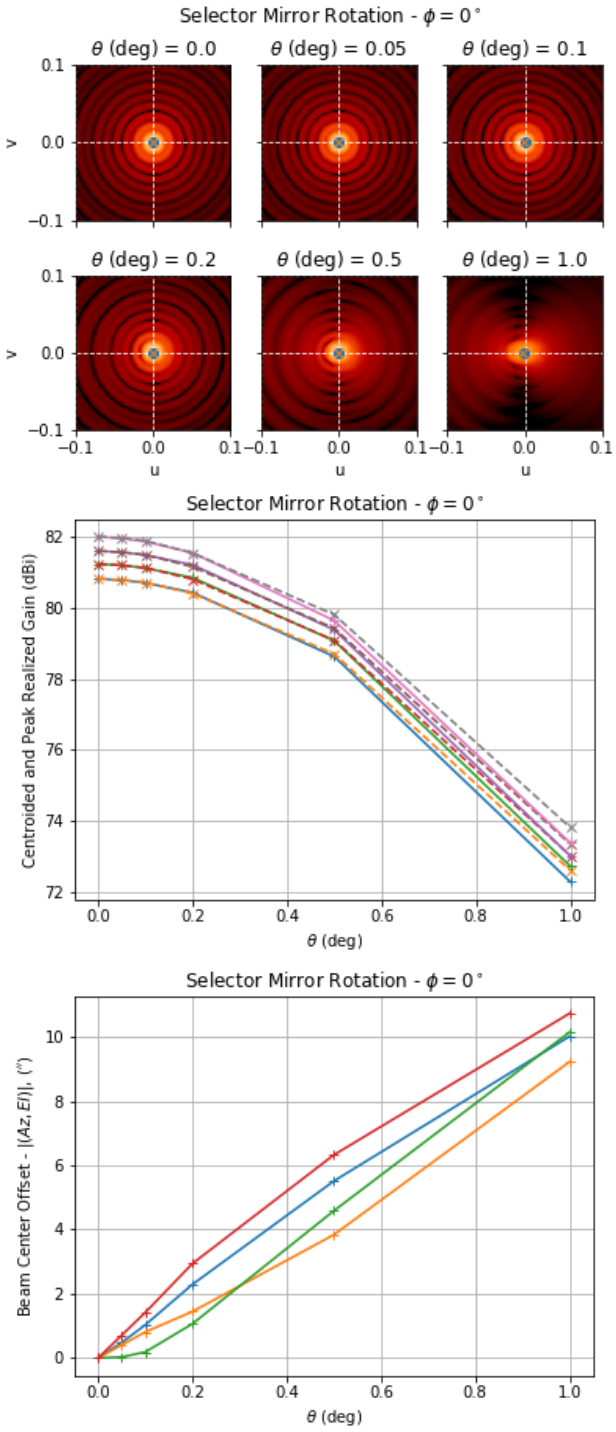

Fig. 11. Far field radiation pattern at 230 GHz (top), peak antenna gain (middle) and position of peak antenna gain (bottom) for 200, 210, 220 and 230 GHz farfield radiation patterns as the angle of the wSMA receiver selector wheel mirror is varied by up to 1°. These variations are used to set the tolerance on the angle of the selector wheel mirror in the wSMA cryostat design.

The GRASP model of the complete SMA optical system in shown in Fig. 10. The model implements physical optics methods for optical surfaces from feed to M3, and physical optics with correction from the physical theory of diffraction for the primary, secondary and key apertures in the optical system.

Key performance measures of the optics derived from the GRASP outputs include the peak gain of the antenna system,

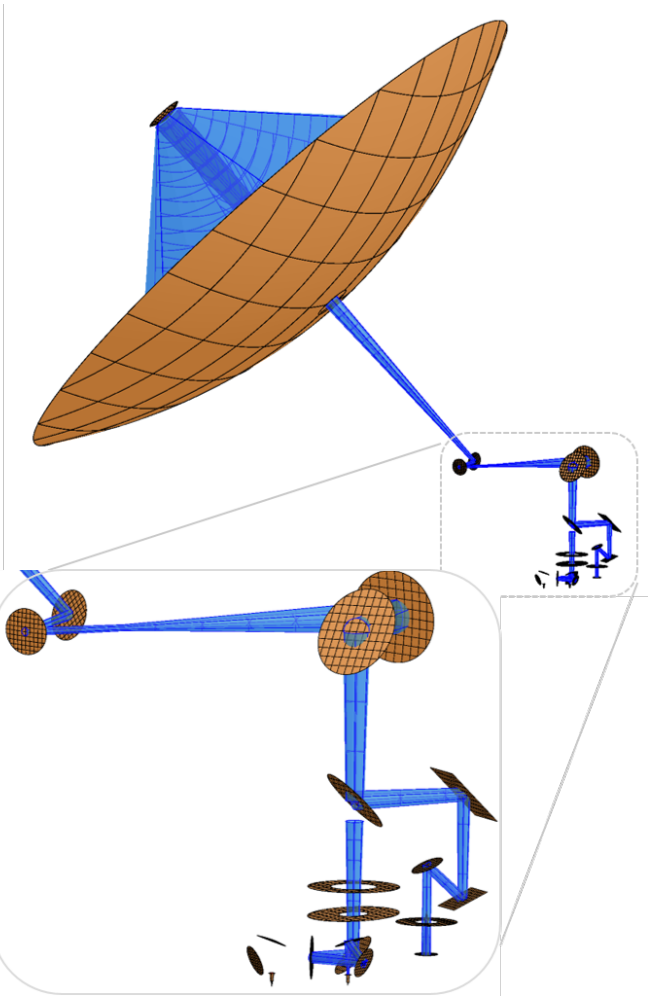

Fig. 10. GRASP model of the SMA antenna, beam waveguide and SMA and wSMA receiver optics, with the 230 GHz Gaussian beam radius shown in blue. An additional view of the wSMA receiver optics model is shown in Fig. 4.

the main beam efficiency (as measured by GRASP's spillover efficiency calculation), peak cross-polarization level, and coalignment between orthogonal polarizations.

In order to derive these measures from the GRASP output, a Python library was written to allow the output fields to be loaded as Numpy arrays [8]. Additional Python functions allowed the peak values and positions of the peaks in the fields to be determined.

The "python-graspfile" Python library for reading and processing GRASP output has been released under the Open Source MIT License, and can be obtained via and is available via the Python Package Index (PyPI) system or GitHub [9].

A. Tolerance Analysis

In order to determine appropriate tolerances for the placement of the receiver cryostat with respect to the telescope and for the positions and angles of the cooled cryostat and receiver optics, the position and angle of each element of the optics was varied individually.

The variation in peak gain and position of peak gain was determined for each variation. Tolerance thresholds were set at variations in position or angle that resulted in a reduction in peak gain of one percent.

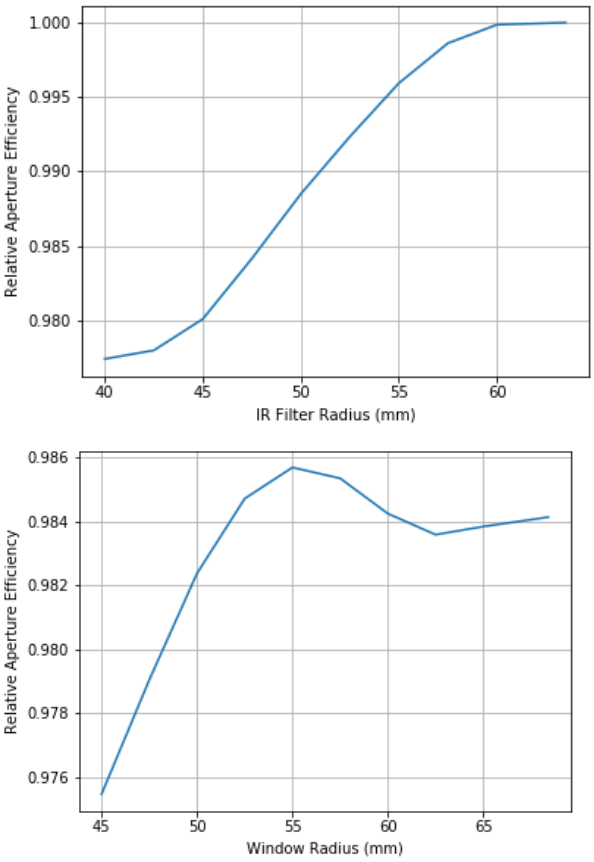

Fig. 12. Beam efficiency from the feed to M6 at 210 GHz as a function if IR Filter radius (top) and cryostat window radius (bottom) for the wSMA Low band receiver. The increase in efficiency at 55 mm window radius is not present at all frequencies within the band, and so the final clear aperture of 52.5 mm radius is a compromise that gives relatively good performance across the band of the Low Band receiver.

These simulations were carried out using the feed design from the SMA 300 GHz receiver. An example of this procedure for the angular tolerance on the wSMA receiver selector wheel mirror position is shown in Fig. 11.

B. IR Aperture and Window Sizing

The minimum size of the IR aperture, which acts as a cold aperture stop in the wSMA optical system, and cryostat window, was determined by running simulations with varying aperture radius, again using the SMA 300 GHz feed design. The minimum IR clear aperture was chosen so that the peak gain was reduced by somewhat less than one percent from the $r = 5w$ case at the lowest specified frequency for the wSMA Low Band receiver (210 GHz).

Once the IR aperture size was fixed, the minimum cryostat window clear aperture was determined by running simulations with fixed IR aperture and varying window size. The minimum window size was chosen to be the minimum size that did not appreciably truncate the beam with the IR aperture in place (total truncation are IR aperture and window < 1%). Beam efficiency results are shown in Fig. 12.

C. Feed Evaluation

Candidate feed designs (described above) were evaluated by comparing the GRASP output for simulations of wSMA receiver optics fed by each design (simulated in CHAMP) with the GRASP simulation output for the complete SMA 200 GHz or SMA 300 GHz receiver. Maximizing the peak gain and beam efficiency were the main criteria.

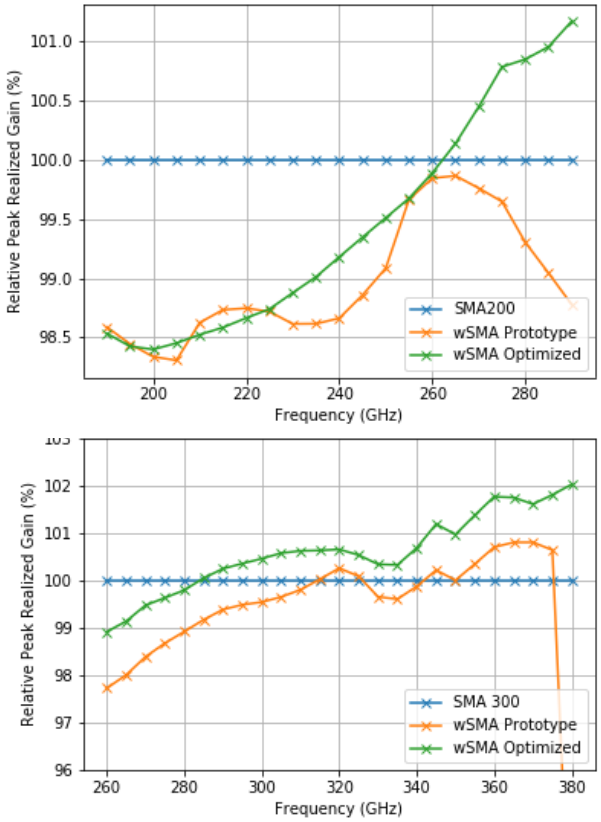

Fig. 13. Relative peak gain of an SMA antenna fed by the wSMA Low Band (top) and High Band (bottom) receivers using the initial prototype feed and the optimized feeds. The baselines for comparison are the existing SMA200 and SMA300 receivers.

The comparison of peak gain for the wSMA receiver fed by the prototype and optimized wSMA feeds with the SMA receivers is shown in Fig. 13. Although the aim was to achieve higher efficiency than the current SMA receivers, for the Low band receiver this would have required too large a window and IR aperture, and thus IR loading on the cryostat. Since the IR aperture forms a ~55 K cold stop in the optical system, the sensitivity of the Low band receiver should not be too badly affected. The High band receiver's narrower beam is not adversely affected by truncation at the IR aperture.

VIII. Conclusion

Two complete prototypes of the wSMA cryostat, receiver optics and receiver feeds are currently being built using the optical design presented in this paper. Following the integration of the wSMA cryostats and receivers, the performance of the optical system and the design will be measured in several ways.

Initial measurements will take place in the laboratory, using a beam scanner system similar to that described in [10]. This will verify that the optical system produces the correct beam, and that the beams of the two receivers are well aligned. Receiver performance measurements will also be carried out.

Following laboratory measurements, the prototype wSMA cryostat and receiver systems will be deployed in at least one SMA antenna at the SMA site on Maunakea. There, tests of the complete system will be made, including on-sky pointing and beam shape measurements, aperture efficiency, and holographic measurements of aperture field distribution of the primary mirror [11] .

REFERENCES

[1] Paul K. Grimes, Raymond Blundell, Scott Paine, John Test, C-Y. Edward Tong, Robert W. Wilson, and Lingzhen Zeng, "The wSMA receivers – a new wideband receiver system for the Submillimeter Array", *28th Int. Symp. Space THz Tech.*, Cologne, Germany, 2017.

[2] Paul K. Grimes, Raymond Blundell, Patrick Leiker, Scott N. Paine, Edward C.-Y. Tong, Robert W. Wilson, and Lingzhen Zeng, "Receivers for the wideband Submillimeter Array", *31st Int. Symp. Space THz Tech.*, Tempe, Arizona, 2020.

[3] S. Paine, Cosmo Papa, R. Louie Leombruno, Xiaolei Zhang, and Raymond Blundell, "Beam Waveguide and Receiver Optics for the SMA," *5th Int. Symp. Space THz Tech.*, Ann Arbor, Michigan, 1994.

[4] Ta-Shing Chu, "An Imaging Beam Waveguide Feed", IEEE Trans. Antennas Propagat., AP-31 614, 1983.

[5] Paul Goldsmith, "Quasioptical Systems", IEEE Press. Piscataway, NJ, 1998.

[6] Christophe Granet and Graeme L. James, "Design of Corrugated Horns: A Primer", IEEE Ant. and Prop. Magazine, 47, 2, 2005.

[7] Lingzhen Zeng, C. Bennett, Chuss, and E. Wollack. "A Low Cross-Polarization Smooth-Walled Horn With Improved Bandwidth." IEEE Transactions on Antennas and Propagation, 58, 4, 2010.

[8] Stéfan van der Walt, S. Chris Colbert and Gaël Varoquaux. The NumPy Array: A Structure for Efficient Numerical Computation, Computing in Science & Engineering, 13, 22-30, 2011.

[9] Paul K. Grimes, "python-graspfile - Python module for reading output and configuration files", https://github.com/Smithsonian/python-graspfile, 2020.

[10] Christensen, Robert D, Ramprasad Rao, T. K Sridharan, and Edward Tong. "Vector Near-field Beam Scanner for the SMA." Proc. SPIE, 9153. 2014.

[11] Sridharan, Tirupati K, Masao Saito, Nimesh A Patel, and Robert D Christensen. "Holographic Surface Setting of the Sub-millimeter Array Antennas." Proc. SPIE, 5495, 2004.